Optimal Control of Coherent Light Scattering for Binary Decision Problems

Dorian Bouchet,[1,*] Lukas M. Rachbauer,[2] Stefan Rotter,[2] Allard P. Mosk,[3] and Emmanuel Bossy[1]
[1]Université Grenoble Alpes, CNRS, LIPhy, 38000 Grenoble, France
[2]Institute for Theoretical Physics, Vienna University of Technology (TU Wien), 1040 Vienna, Austria
[3]Nanophotonics, Debye Institute for Nanomaterials Science and Center for Extreme Matter and Emergent Phenomena, Utrecht University, P.O. Box 80000, 3508 TA Utrecht, Netherlands

(Received 26 July 2021; accepted 18 November 2021; published 17 December 2021)

Because of quantum noise fluctuations, the rate of error achievable in decision problems involving several possible configurations of a scattering system is subject to a fundamental limit known as the Helstrom bound. Here, we present a general framework to calculate and minimize this bound using coherent probe fields with tailored spatial distributions. As an example, we experimentally study a target located in between two disordered scattering media. We first show that the optimal field distribution can be directly identified using a general approach based on scattering matrix measurements. We then demonstrate that this optimal light field successfully probes the presence of the target with a number of photons that is reduced by more than 2 orders of magnitude as compared to unoptimized fields.

DOI: 10.1103/PhysRevLett.127.253902

Many sensing applications rely on the detection of targets embedded within disordered or engineered materials. For instance, interferometric techniques are currently being developed to detect the presence of single particles within biological specimens based on coherent light scattering [1,2]. Coherent beams are also used to detect the presence of defects in nanofabricated samples such as integrated circuits [3,4]. In such experiments, and more generally for all decision problems involving several possible configurations of a given scattering system, the rate of error is fundamentally limited by quantum noise fluctuations [5,6], which usually appear in measured data as shot noise. This limit, which predicts high rates of error for measurements performed in low-light conditions, represents a central obstacle for the development of nondestructive high-speed sensing techniques. Different strategies have been devised to address this challenge, notably by finding optimal and robust receivers for coherent states [6–11] and by adopting quantum illumination schemes [12–14]; however, all these approaches are primarily applied to scattering systems with simple permittivity distributions.

When interacting with complex media such as disordered media or engineered nanomaterials, light is usually absorbed and scattered multiple times, resulting in the formation of complex interference patterns. Despite this difficulty, it has been shown that the propagation of light in such media can be controlled by spatially modulating the incident field using wavefront shaping protocols [15–17]. These methods have opened up the possibility to optimally deposit and store energy in or behind scattering materials [18–24]. Integrated in a framework based on estimation theory, wavefront shaping also enables the generation of optimal fields that maximize the Fisher information retrieved from complex scattering systems, thus allowing one to precisely estimate small variations in the value of continuous parameters [25,26]. The question then arises as to how wavefront shaping can be used for target detection and, more generally, for any decision problem in which a number of hypotheses are formulated and an experiment is conducted to decide on which hypothesis is true. This question is especially important in the development of optical microscopes optimized for (nonimaging) decision tasks, as promoted by the advent of approaches based on deep learning algorithms [27–31].

In this Letter, we identify and experimentally generate coherent light fields that are optimally shaped for decision problems involving two possible configurations of a complex scattering system. To this end, we introduce the *discrimination operator*, which allows one to directly identify the spatial distribution of the field that minimizes the rate of error due to quantum noise fluctuations. We first show that this operator can be readily constructed from the knowledge of the scattering matrices describing each configuration of the system. We then illustrate this approach experimentally by generating a light field that is optimized to detect the presence of a target hidden in between two disordered scattering media. This field is shown to optimally interact with the target, despite its complex environment. Finally, we demonstrate that this optimal field successfully probes the presence of the hidden target in low-light conditions, with a number of photons that is reduced by more than 2 orders of magnitude as compared to unoptimized fields. These results, which connect quantum detection theory to wavefront shaping, establish a new benchmark to assess and improve the

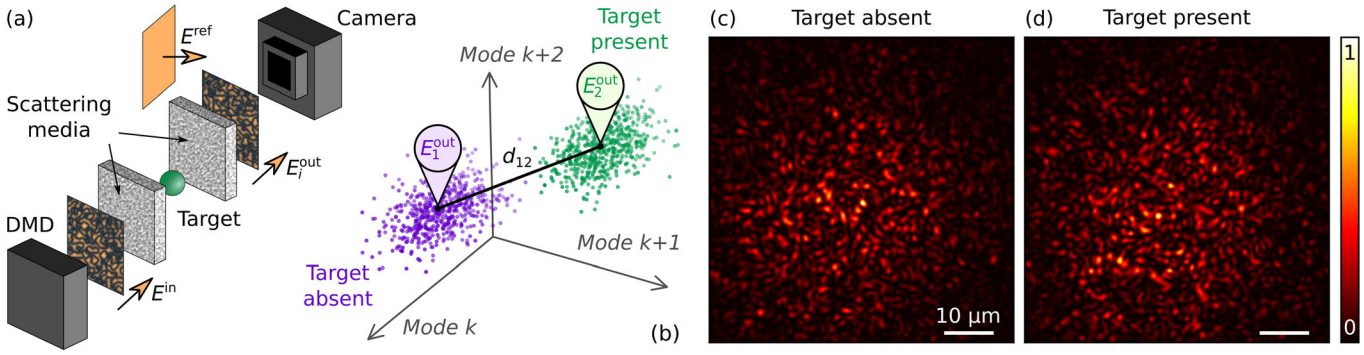

FIG. 1. (a) Representation of the experiment, which consists in optically probing the presence of a target (3 μm in diameter) located between two scattering media. The system is illuminated with an incident field that is spatially modulated using a digital micromirror device (DMD). The field that comes out of the system is measured by a camera in N spatial modes using a homodyne scheme. (b) The measured field spans a complex N-dimensional space. The expectation value of the field depends on the presence of the target, and its variance is ultimately limited by quantum noise fluctuations. The incident field optimally probes the presence of the target when the statistical distance d_{12} is maximized. (c),(d) Intensity distributions experimentally measured with the optimal incident field when the hidden target is (c) absent and (d) present. Because of complex absorption and scattering processes involved within the system, these distributions appear as speckle patterns. Despite this complexity, the optimal light field is strongly affected by the presence of the target, which allows us to detect this target with a minimum rate of error.

performances of sensing and classification techniques using structured illumination.

We consider an arbitrarily complex scattering system that can take two distinct configurations with probabilities π_1 and π_2. Detecting the presence of a target included within a given scattering medium [Fig. 1(a)] constitutes a typical example of such a situation: the target can either be absent (hypothesis H_1) or present (hypothesis H_2). To decide on which hypothesis is true, we apply a measurement to the scattering system and we choose a hypothesis based on a decision criterion, resulting in a probability of error P_{err}. This probability can be minimized by optimizing over both the decision criterion and the positive operator-valued measure (POVM) describing the measurement process. The minimum probability of error P_H, which is limited only by quantum noise fluctuations, is calculated from the trace distance between the two quantum states associated with each hypothesis—a result known as the Helstrom bound [5,6]. This general formalism can be applied to the case of a probe field in a coherent state described by the coefficients $\{E_1^{\mathrm{in}}, \ldots, E_M^{\mathrm{in}}\}$ in M spatial modes. After interacting with the scattering system, such an incident state produces an outgoing state that is similarly described by the coefficients $\{E_{i,1}^{\mathrm{out}}, \ldots, E_{i,N}^{\mathrm{out}}\}$ in N spatial modes, where the subindex i denotes the configuration of the scattering system interacting with the field (if H_1 is true $i = 1$, and if H_2 is true $i = 2$). Note that these coefficients, defined here as expectation values (calculated over quantum noise fluctuations) of the complex field operator, can equivalently be interpreted as describing the complex classical field. The Helstrom bound is then simply expressed by [5]

$$P_H = \frac{1}{2}\left[1 - \sqrt{1 - 4\pi_1\pi_2 \exp\left(-n d_{12}^2\right)}\right], \tag{1}$$

where n is the number of incident photons and d_{12} is a statistical distance expressed by

$$d_{12}^2 = \frac{1}{n}\sum_{k=1}^{N} |E_{2,k}^{\mathrm{out}} - E_{1,k}^{\mathrm{out}}|^2. \tag{2}$$

The distance d_{12} quantifies the overlap between two different outgoing states [Fig. 1(b)], as created by the interaction of a single photon with each of the two possible configurations of the scattering system. This distance consequently drives the exponential decay of the probability of error that is achieved when both the POVM and the decision criterion are optimized. Indeed, in the asymptotic limit ($n \gg d_{12}^{-2}$), the Helstrom bound decays exponentially with n, with a decay constant given by d_{12}^2. Equation (2) also explicitly shows that, for a binary decision problem, the contribution of each outgoing mode simply sums up to set the Helstrom bound.

Far-field wavefront shaping techniques enable us to generate incident states with custom spatial distributions [15]. Here, our goal is to identify the optimal field distribution that minimizes the Helstrom bound for any given number n of incident photons, which entails maximizing d_{12}^2 over all possible incident states. For this purpose, we introduce the scattering matrices S_1 and S_2 [17], which connect incident to outgoing states under the respective hypotheses (target being absent or present). These scattering matrices are supposed to be known, either by *ab initio* calculations or by prior measurements. Conveniently writing Eq. (2) in bra-ket notation $n d_{12}^2 = \langle E_2^{\mathrm{out}} - E_1^{\mathrm{out}} | E_2^{\mathrm{out}} - E_1^{\mathrm{out}} \rangle$, and introducing the linear relation defining the S matrix $|E_i^{\mathrm{out}}\rangle = S_i |E^{\mathrm{in}}\rangle$, we obtain the following quadratic form (see Supplemental Material [32], Sec. S1.1):

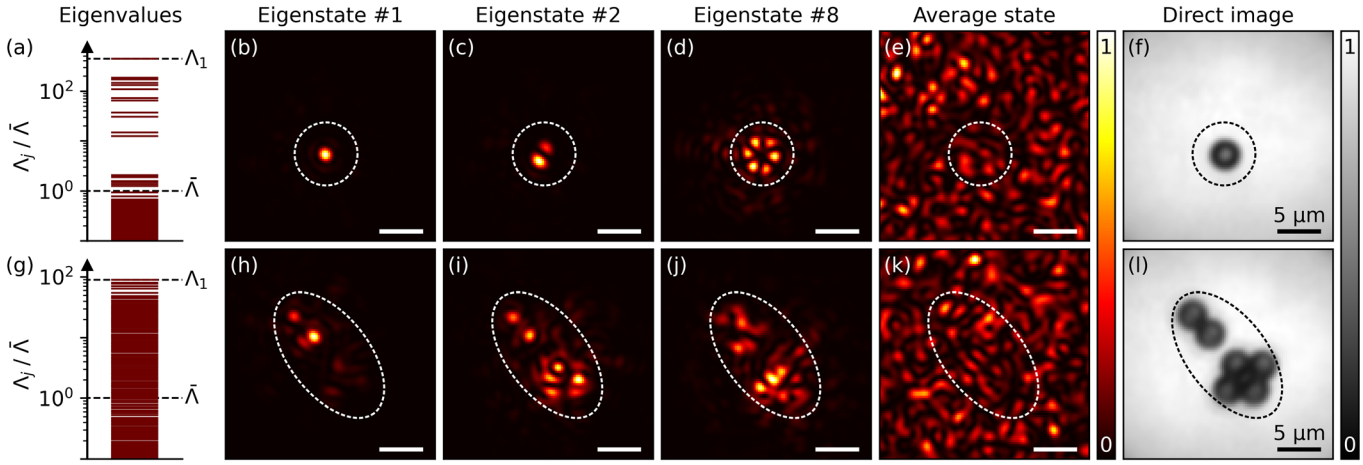

FIG. 2. (a) Eigenvalues Λ_j of the discrimination operator, normalized by the average value $\bar{\Lambda}$ (the averaging is performed over all possible incident states). Small eigenvalues (associated with measurement noise) are closely spaced and appear as a continuum due to the finite thickness of the lines, while large eigenvalues (associated with eigenstates that significantly interact with the target) appear as discrete lines. (b)–(e) Intensity distribution in the target plane measured for a few representative eigenstates—including (b) the first eigenstate (i.e., the optimal state), (c) the second eigenstate, and (d) the eighth eigenstate—as well as for (e) the average state (defined as an equally weighted linear superposition of all eigenstates). These distributions were measured in the absence of the target, and without the scattering medium located between the target and the camera. (f) Image of the target (a single bead) measured under spatially incoherent illumination. (g)–(l) Analogous to (a)–(f) for a target composed of six beads.

$$d_{12}^2 = \langle \mathcal{E}^{\text{in}} | D_{12} | \mathcal{E}^{\text{in}} \rangle, \tag{3}$$

where $|\mathcal{E}^{\text{in}}\rangle = n^{-1/2}|E^{\text{in}}\rangle$ is the normalized incident state and where $D_{12} = (S_2 - S_1)^\dagger (S_2 - S_1)$ is a Hermitian operator that we refer to as the *discrimination operator*. Among the M eigenvalues of D_{12}, which all lie in the interval [0;4], the largest one is of specific interest as it gives the maximum achievable value of d_{12}^2, which is reached by illuminating the scattering system with the corresponding eigenstate. This general approach thus allows one to minimize the Helstrom bound from the knowledge of the scattering matrices S_1 and S_2, regardless of the complexity of absorption and scattering processes that are involved within the system [Figs. 1(c) and 1(d)].

In order to investigate the properties of the discrimination operator experimentally, we study a target (a polystyrene bead with a diameter of 3 μm) located on a glass coverslip, that we place in between ground glass diffusers [Fig. 1(a), see also Supplemental Material [32], Secs. S3 and S4]. This scattering system is illuminated using coherent light at a wavelength $\lambda = 532$ nm. To characterize the system through transmission matrix measurements [37], we modulate the amplitude and the phase of the incident field with a digital micromirror device (DMD) using Lee holography [38], and we measure both quadratures of the outgoing field with a camera using off-axis holography [39]. In this way, we control $M = 1735$ incident modes and $N = 2617$ outgoing modes, allowing us to acquire two (subunitary) transmission matrices S_1 and S_2 measured with the target present and absent from the field of view, respectively.

The knowledge of these matrices allows us to construct the discrimination operator D_{12}, and thus to identify the optimal incident state via an eigenvalue decomposition of D_{12}. To quantitatively assess the benefits of operating with the optimal state instead of unoptimized ones, we can study the M eigenvalues of D_{12}, which we sort in descending order [Fig. 2(a)]. Using this convention, the maximal value of d_{12}^2 is given by the first eigenvalue Λ_1, which we compare to the value of d_{12}^2 averaged over all possible incident states. This average value $\bar{\Lambda} = \text{Tr}(D_{12})/M$ is exactly reached for an equally weighted linear superposition of all eigenstates, that we refer to as the average state. In our experiment, using the optimal state instead of the average one is shown to drastically enhance d_{12}^2, with a ratio $\Lambda_1/\bar{\Lambda}$ of the order of 400. This implies that the number of incident photons needed to reach a given probability of error is smaller by more than 2 orders of magnitude with the optimal state.

In order to acquire a better understanding of the field distribution within the system, we kept the first diffuser (located between the DMD and the target) but temporarily removed the second diffuser (located between the target and the camera). In this configuration, the camera directly images the plane of the target, thereby allowing us to visualize how the different eigenstates interact with the target [Figs. 2(b)–2(f)]. We can see that the first eigenstate optimally interacts with the target by generating a strong focus at its position. Remarkably, the intensity distribution of all eigenstates that strongly interact with the target (those associated with the largest eigenvalues) have a structured aspect that resemble those of Laguerre-Gaussian modes

[Figs. 2(b)–2(d), see also Supplemental Material [32], Sec. S5.1), as opposed to the specklelike distribution generated by the average state [Fig. 2(e)]. We specifically observe that the 12 largest eigenvalues are significantly above the noise floor, a number that matches the number of existing optical modes in the area covered by the target. Several of these eigenvalues are close to be degenerate, as explained by symmetries in the intensity distributions generated by the eigenstates.

The generality of our formalism allows us to identify optimal states not only in the case of a single bead but also for more complicated targets. As an example, we study the case of a target composed of a cluster of six beads [Figs. 2(g)–2(l)]. In this case, the eigenstates that significantly interact with the target [Figs. 2(h)–2(j), see also Supplemental Material [32], Sec. S5.2] are all characterized by complicated intensity distributions that cannot be easily predicted without the knowledge of the discrimination operator. These results illustrate the fact that optimal states do not necessarily focus light everywhere onto extended targets, but instead provide one with the unique optimal solutions that generally minimize the Helstrom bound, taking into account absorption as well as all single and multiple scattering effects (including, e.g., strong coupling effects occurring between a light field and the dipoles induced within a strongly scattering target). However, for such an extended target, the eigenvalue distribution appears as a continuum [Fig. 2(g)], which prevents us from easily relating the number of large eigenvalues to the spatial extent of the target.

While we introduced the discrimination operator to minimize the Helstrom bound, which can be reached only with an optimal detection scheme, it is also the relevant operator to find optimal incident fields in the case of Gaussian receivers, which are sub-optimal but widely used due to their simplicity [6]. Indeed, a simple homodyne scheme is optimal among all available Gaussian receivers [40], whereas implementing an optimal detection scheme—such as a Dolinar receiver [7]—typically requires low-noise time-resolved photon detection along with an excellent interferometric stability. With the homodyne detection scheme implemented in our experiment (which is shot-noise limited), measured field quadratures follow a Gaussian distribution of variance $\sigma^2 = 1/2$ (see Supplemental Material [32], Sec. S2.1). For two hypotheses with equal *a priori* probabilities ($\pi_1 = \pi_2 = 0.5$), the theoretical probability of error associated with this Gaussian receiver is then expressed by (see Supplemental Material [32], Sec. S2.2),

$$P_G = \frac{1}{2}\mathrm{erfc}\left(\sqrt{\frac{nd_{12}^2}{8\sigma^2}}\right). \tag{4}$$

This expression shows that accessing the discrimination operator allows one to minimize not only the Helstrom bound but also the probability of error associated with homodyne detection schemes, as they are both governed by the statistical distance d_{12}. This is experimentally demonstrated by performing measurements in low-light conditions, using a variable attenuator to gradually change the number of incident photons. The presence of the bead located in between diffusers is tested by illuminating the system with either the optimal incident state ($d_{12}^2 = \Lambda_1$) or with the average state ($d_{12}^2 = \bar{\Lambda}$). Measured data are then processed using the likelihood-ratio test (see Supplemental Material [32], Sec. S2.3), which is theoretically optimal [41]. The resulting rate of error observed over $N_{\mathrm{rep}} = 4000$ measurements is shown in Fig. 3 as a function of the number n of incident photons. The measured rate of error, which exponentially decreases with n, is characterized by a decay constant that is larger by more than 2 orders of magnitude for the optimal state (red points) as compared to the average one (blue points). Consequently, with the optimal state, far fewer photons are needed to accurately detect the presence of the target. Measured rates of error are only slightly higher than theoretical values predicted by Eq. (4) (solid lines), a difference that is due to a slightly sub-optimal decision criterion—the likelihood-ratio test requires unbiased estimates of the field expectation values that are difficult to obtain in low-light conditions. Finally, the Helstrom bound calculated using Eq. (1) is similarly reduced when the optimal state is used instead of the average one (dashed lines), although with a lower overall error rate.

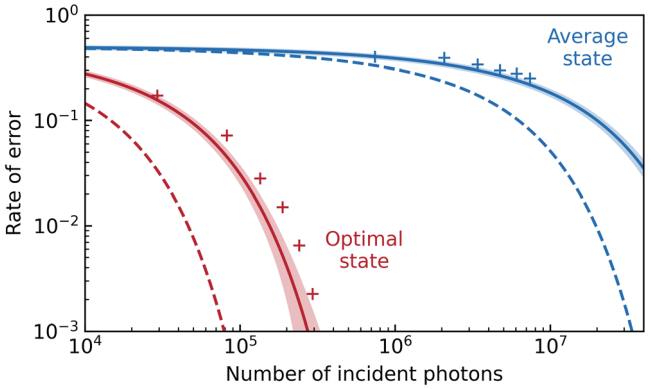

FIG. 3. Rate of error as a function of the number of incident photons for the average state (blue) and the optimal state (red). In both cases, the experimentally observed error rates (data points) are compared to the theoretical values associated with our homodyne setup (solid lines) and to the Helstrom bound (dashed lines). Shaded areas represent 95.4% confidence intervals, taking into account only the statistical error caused by the finite number of measurements ($N_{\mathrm{rep}} = 4000$). Note that, while we illuminate the system with up to 7.4×10^6 photons, many photons are scattered out of the field of view by the diffusers. As a consequence, we only detect up to 140 photons over the area covered by the camera sensor.

Whereas we measured only subparts of the full S matrix in our experiments, as usually done in optics [37,42]—it is also instructive to discuss the ideal case of unitary

scattering matrices ($S_i^{-1} = S_i^\dagger$). This is achieved for systems without gain or loss (e.g., multimode fibers [43,44]), if one has access to all existing incident and outgoing optical modes. The eigenstates of D_{12} are then solutions of a generalized linear eigenvalue problem, in the same way as scattering invariant modes [45]. In this unitary limit, the optimal state along with all other eigenstates of D_{12} thus share a remarkable property: they all produce outgoing fields that are independent of which of the two scattering systems they interact with, except for a global phase factor which affects all outgoing modes and which contains all available information (see Supplemental Material [32], Sec. S1.2). Nevertheless, as could be expected from the subunitarity of the measured transmission matrices, this property is not observed in our experiment [see Figs. 1(c) and 1(d)].

To summarize, we demonstrated how to spatially modulate light fields in order to optimally discriminate between different configurations of a complex scattering system. To this end, we introduced the discrimination operator D_{12}, which quantifies the amount of information produced by any perturbation of a discrete observable. We experimentally showed how to use this operator for generating light states that are optimally tailored to detect a target located inside a disordered medium even in low-light conditions. These results open up new perspectives to improve the performances of nanophotonic sensing devices based, e.g., on photonic crystal waveguides [46], metasurfaces [47,48], or cavities [49]. The orthonormal basis formed by the eigenstates of D_{12} is also well suited to analyze experiments based on time-reversed adapted perturbation [50–53], which in turn suggests interesting experimental approaches to generate optimal states. Moreover, by associating scattering matrix measurements with advanced optimization procedures [54], optimal states could potentially be identified for decision problems involving more than two configurations as well as to composite hypotheses problems [5,41]. Interestingly, our results might also find applications in cryptography, notably to identify physical unclonable keys that are the most difficult to reproduce [55,56]. Finally, the formalism developed in our work suggests a new path to study complex scattering systems using quantum illumination [13]. In this perspective, the use of squeezed states of light emerges as a promising approach [57,58].

The authors thank Irène Wang for insightful discussions, and Philippe Moreau for technical support. This work was supported by the European Research Council (ERC) within the H2020 program (Grant No. 681514-COHERENCE), by the Nederlandse Organisatie voor Wetenschappelijk Onderzoek NWO (Vici 68047618) and by the Austrian Science Fund (FWF) under Project No. P32300 (WAVELAND).

*dorian.bouchet@univ-grenoble-alpes.fr

[1] R. W. Taylor and V. Sandoghdar, Nano Lett. **19**, 4827 (2019).
[2] G. Young and P. Kukura, Annu. Rev. Phys. Chem. **70**, 301 (2019).
[3] N. G. Orji, M. Badaroglu, B. M. Barnes, C. Beitia, B. D. Bunday, U. Celano, R. J. Kline, M. Neisser, Y. Obeng, and A. E. Vladar, Nat. Electron. **1**, 532 (2018).
[4] K. A. Brown, S. Brittman, N. Maccaferri, D. Jariwala, and U. Celano, Nano Lett. **20**, 2 (2020).
[5] C. W. Helstrom, *Quantum Detection and Estimation Theory* (Academic Press, New York, 1976).
[6] C. Weedbrook, S. Pirandola, R. García-Patrón, N. J. Cerf, T. C. Ralph, J. H. Shapiro, and S. Lloyd, Rev. Mod. Phys. **84**, 621 (2012).
[7] R. L. Cook, P. J. Martin, and J. M. Geremia, Nature (London) **446**, 774 (2007).
[8] F. E. Becerra, J. Fan, G. Baumgartner, J. Goldhar, J. T. Kosloski, and A. Migdall, Nat. Photonics **7**, 147 (2013).
[9] D. Sych and G. Leuchs, Phys. Rev. Lett. **117**, 200501 (2016).
[10] M. A. Solís-Prosser, M. F. Fernandes, O. Jiménez, A. Delgado, and L. Neves, Phys. Rev. Lett. **118**, 100501 (2017).
[11] M. T. DiMario and F. E. Becerra, Phys. Rev. Lett. **121**, 023603 (2018).
[12] S. Lloyd, Science **321**, 1463 (2008).
[13] S. Pirandola, B. R. Bardhan, T. Gehring, C. Weedbrook, and S. Lloyd, Nat. Photonics **12**, 724 (2018).
[14] R. Nair and M. Gu, Optica **7**, 771 (2020).
[15] A. P. Mosk, A. Lagendijk, G. Lerosey, and M. Fink, Nat. Photonics **6**, 283 (2012).
[16] R. Horstmeyer, H. Ruan, and C. Yang, Nat. Photonics **9**, 563 (2015).
[17] S. Rotter and S. Gigan, Rev. Mod. Phys. **89**, 015005 (2017).
[18] I. M. Vellekoop and A. P. Mosk, Phys. Rev. Lett. **101**, 120601 (2008).
[19] M. Kim, Y. Choi, C. Yoon, W. Choi, J. Kim, Q.-H. Park, and W. Choi, Nat. Photonics **6**, 581 (2012).
[20] S. M. Popoff, A. Goetschy, S. F. Liew, A. D. Stone, and H. Cao, Phys. Rev. Lett. **112**, 133903 (2014).
[21] X. Cheng and A. Z. Genack, Opt. Lett. **39**, 6324 (2014).
[22] P. Ambichl, A. Brandstötter, J. Böhm, M. Kühmayer, U. Kuhl, and S. Rotter, Phys. Rev. Lett. **119**, 033903 (2017).
[23] M. Durand, S. M. Popoff, R. Carminati, and A. Goetschy, Phys. Rev. Lett. **123**, 243901 (2019).
[24] N. Bender, A. Yamilov, A. Goetschy, H. Yilmaz, C. W. Hsu, and H. Cao, arXiv:2105.13417.
[25] D. Bouchet, R. Carminati, and A. P. Mosk, Phys. Rev. Lett. **124**, 133903 (2020).
[26] D. Bouchet, S. Rotter, and A. P. Mosk, Nat. Phys. **17**, 564 (2021).
[27] E. Hershko, L. E. Weiss, T. Michaeli, and Y. Shechtman, Opt. Express **27**, 6158 (2019).
[28] M. R. Kellman, E. Bostan, N. A. Repina, and L. Waller, IEEE Trans. Comput. Imag. **5**, 344 (2019).
[29] A. Muthumbi, A. Chaware, K. Kim, K. C. Zhou, P. C. Konda, R. Chen, B. Judkewitz, A. Erdmann, B. Kappes, and R. Horstmeyer, Biomed. Opt. Express **10**, 6351 (2019).

[30] P. d. Hougne, M. F. Imani, A. V. Diebold, R. Horstmeyer, and D. R. Smith, Adv. Sci. **7**, 1901913 (2020).
[31] R. Horisaki, R. Horisaki, Y. Okamoto, and J. Tanida, Opt. Lett. **45**, 3131 (2020).
[32] See Supplemental Material at http://link.aps.org/supplemental/10.1103/PhysRevLett.127.253902 for detailed derivations and additional experimental results, which includes Refs. [33–36].
[33] R. Loudon, *The Quantum Theory of Light* (Oxford University Press, Oxford, 2000).
[34] J. W. Goodman, *Statistical Optics* (John Wiley & Sons, Hoboken, 2015).
[35] P. Pai, J. Bosch, and A. P. Mosk, OSA Continuum **3**, 637 (2020).
[36] M. Mirhosseini, O. S. Magaña-Loaiza, C. Chen, B. Rodenburg, M. Malik, and R. W. Boyd, Opt. Express **21**, 30196 (2013).
[37] S. M. Popoff, G. Lerosey, R. Carminati, M. Fink, A. C. Boccara, and S. Gigan, Phys. Rev. Lett. **104**, 100601 (2010).
[38] W.-H. Lee, Appl. Opt. **13**, 1677 (1974).
[39] E. Cuche, P. Marquet, and C. Depeursinge, Appl. Opt. **39**, 4070 (2000).
[40] M. Takeoka and M. Sasaki, Phys. Rev. A **78**, 022320 (2008).
[41] H. L. V. Trees, K. L. Bell, and Z. Tian, *Detection Estimation and Modulation Theory, Part I* (John Wiley & Sons, Hoboken, 2013).
[42] H. Yu, T. R. Hillman, W. Choi, J. O. Lee, M. S. Feld, R. R. Dasari, and Y. K. Park, Phys. Rev. Lett. **111**, 153902 (2013).
[43] M. Plöschner, T. Tyc, and T. Čižmár, Nat. Photonics **9**, 529 (2015).
[44] M. W. Matthès, Y. Bromberg, J. de Rosny, and S. M. Popoff, Phys. Rev. X **11**, 021060 (2021).
[45] P. Pai, J. Bosch, M. Kühmayer, S. Rotter, and A. P. Mosk, Nat. Photonics **15**, 431 (2021).
[46] A. Bag, M. Neugebauer, U. Mick, S. Christiansen, S. A. Schulz, and P. Banzer, Nat. Commun. **11**, 2915 (2020).
[47] T. A. W. Wolterink, R. D. Buijs, G. Gerini, A. F. Koenderink, and E. Verhagen, Nanophotonics **10**, 1723 (2021).
[48] R. D. Buijs, T. A. W. Wolterink, G. Gerini, E. Verhagen, and A. F. Koenderink, Adv. Opt. Mater. **9**, 2100435 (2021).
[49] M. del Hougne, S. Gigan, and P. del Hougne, Phys. Rev. Lett. **127**, 043903 (2021).
[50] M. Fink, D. Cassereau, A. Derode, C. Prada, P. Roux, M. Tanter, J.-L. Thomas, and F. Wu, Rep. Prog. Phys. **63**, 1933 (2000).
[51] E. H. Zhou, H. Ruan, C. Yang, and B. Judkewitz, Optica **1**, 227 (2014).
[52] C. Ma, X. Xu, Y. Liu, and L. V. Wang, Nat. Photonics **8**, 931 (2014).
[53] H. Ruan, T. Haber, Y. Liu, J. Brake, J. Kim, J. M. Berlin, and C. Yang, Optica **4**, 1337 (2017).
[54] D. Bouchet, J. Seifert, and A. P. Mosk, Opt. Lett. **46**, 254 (2021).
[55] R. Pappu, B. Recht, J. Taylor, and N. Gershenfeld, Science **297**, 2026 (2002).
[56] R. Uppu, T. A. W. Wolterink, S. A. Goorden, B. Chen, B. Škorić, A. P. Mosk, and P. W. H. Pinkse, Quantum Sci. Technol. **4**, 045011 (2019).
[57] U. L. Andersen, T. Gehring, C. Marquardt, and G. Leuchs, Phys. Scr. **91**, 053001 (2016).
[58] G. Chesi, S. Olivares, and M. G. A. Paris, Phys. Rev. A **97**, 032315 (2018).